Research Article • DOI: 10.2478/amst-2019-0024 AMST • 44(4) • 2020 • 145–154

Advances in Manufacturing Science and Technology

Determination of contact pattern for double enveloping worm gear

Piotr Polowniak*, Mariusz Sobolak, Adam Marciniec

The Faculty of Mechanical Engineering and Aeronautics, Rzeszow University of Technology
al. Powstańców Warszawy 12 35-959 Rzeszów, Poland

Abstract ***The paper presents the method of determining geometric contact pattern by using the direct computer-aided design (CAD) method for ideal globoid worm gear in which mounting deviations are considered. The tooth contact analysis was performed for all cycle of worm rotation. Based on the results of temporary contact pattern, graphical characteristics of the contact area size depending on worm position were made. A complete analysis of the correctness of gear meshing can be obtained based on presented method. If the worm or worm wheel is incorrectly designed in terms of the geometry, the meshing simulation of CAD models can indicate the collision. Geometric contact pattern analyses were made at two pressure angles of ideal gear. The analysis of the influence of mounting deviations was done against one selected pressure angle and one gear position.***

Keywords *globoid worm gear, contact pattern, CAD environment, tooth contact analysis, meshing simulation*

1. Introduction

The globoid worm drive was initially invented in 1765 by H. Hindley [1,2]. In the beginning of the 20th century, Samuel I. Cone proposed to manufacture an hourglass using a lathe tool with a straight blade. A meshing worm gear is manufactured using an hourglass hob similar to an hourglass worm [3]. This type of drive is characterized by double lines and a multi-tooth contact. It has a greater transmission efficiency, smaller size, and heavier load capacity in comparison with a cylindrical worm drive. Moreover, the forming characteristics of the lubricant layer between the teeth are quite good [4]. However, globoid worm gear is sensitive to manufacturing and misalignment errors which are a great adverse effect [5]. Because of the advantages of this type of gear, industries started to use them in wider applications very rapidly. The development history of worm drives was reviewed and their characteristics and applications were introduced [6]. In addition, a systematic classification table of worm gears was proposed. Also, the development trends and research hotspots of a worm drive were pointed out. It was stated that a double-enveloping hourglass worm drive and a high-precision heavy-load worm drive will be the development priorities in the future [6].

Double enveloping worm drives have been the subject of research by numerous scientists. The research on mathematical modeling and analyses of the gears [7,8], the introduction of modifications [9,10], surface analyses [11,12], the development of new types of globoid worm gears [13,14], and manufacturing methods [15,16] are still ongoing. Chen and Tsay [7] studied the hourglass worm gear composed of a ZN-type hourglass worm generated by straight-edged blade cutters and a worm wheel generated by worm-type hourglass hob cutters. Mohan and Shunmugam [8] developed a geometrical simulation of worm wheel tooth generation using the different axial section profiles of the worm representing the hob cutting edges. Further, Simon [13,14] has proposed a new type of double-enveloping worm gear drive. The gear tooth surface of the worm gear is smooth, and is shaped by a flying tool whose cutting edge is identical to the profile of the entering edge of the worm. Chen et al. [17] presented a novel hourglass worm drive named as involute gear meshing with a planar-enveloping hourglass worm drive. They studied the theory of tooth contact analysis of the hourglass worm drive, which is developed based on numerical and finite element analyses. Zhao et al. [18] established the meshing geometry of a modified globoidal worm drive. The modification parameters included the center distance, transmission ratio, and cutter frame height when machining

*Corresponding author: Piotr Polowniak
*E-mail: ppolowniak@prz.edu.pl

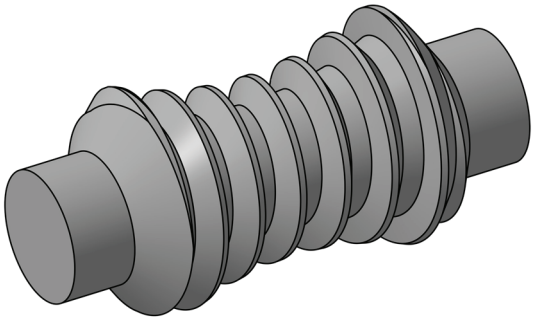

Figure 1. Model of globoid worm.

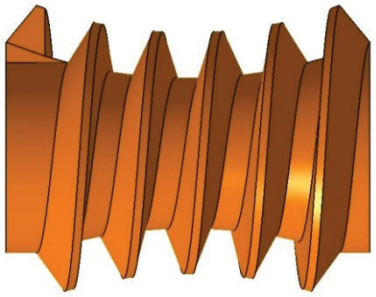

Figure 2. Globoid machining worm.

the worm. A full mathematical description of the tooth flank surface of the globoid worm and worm wheel was presented in the paper [19]. The axial section of the worm was established as a straight line and worm wheel was generated using a hob cutter, which is identical to a TA worm. An investigation into a CAD modeling method for enveloping the surface parts including a double-enveloping surface is still going on [20,21]. A concept of CAD modeling of a worm and worm wheel tooth surface was presented in a demonstrative way by means of drawing schemes and short descriptions [22,23]. A detailed description of the modeling of the globoid worm and worm wheel in CAD environment was presented in the papers [24-26]. CAD models can be used in the applications: (1) in analysis of the geometrical contact pattern in a CAD environment [27], (2) to carry out FEM (Finite Element Method) analysis, and (3) to manufacture real parts or to prototype models through the rapid prototyping technique [28,29].

The investigation of double enveloping worm gear is mainly focused on either mathematical meshing analysis or manufacturing aspects. Furthermore, the meshing analyses are carried out in the range of effective worm length. But, CAD model of the globoid worm considers the whole thread length, which allows a complete analysis of the correctness of meshing. After modeling the worm and worm wheel in CAD environment [24–26], the aim of this study is to perform analyses of geometric contact pattern determined by means of the direct CAD method. The method of determining geometric contact pattern allows establishing its shape and area. The analyses consider the influence of mounting deviations on the contact pattern. Contact pattern analyses show that the globoid worm gear characterizes by multi-tooth contact. The surface area of the first contact pattern in the entire cycle of worm rotation is the greatest, and the contact pattern is smaller for each subsequent fragment of helical surface. It can be found that the double-enveloping worm gear drive is sensitive to tolerances and mounting deviations. It needs precise manufacturing and accurate alignment.

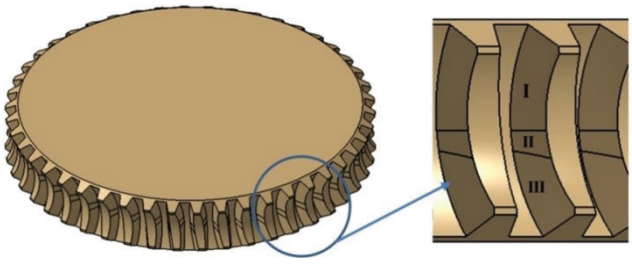

Figure 3. Model of worm wheel with separate detail and marked regions of the tooth flank.

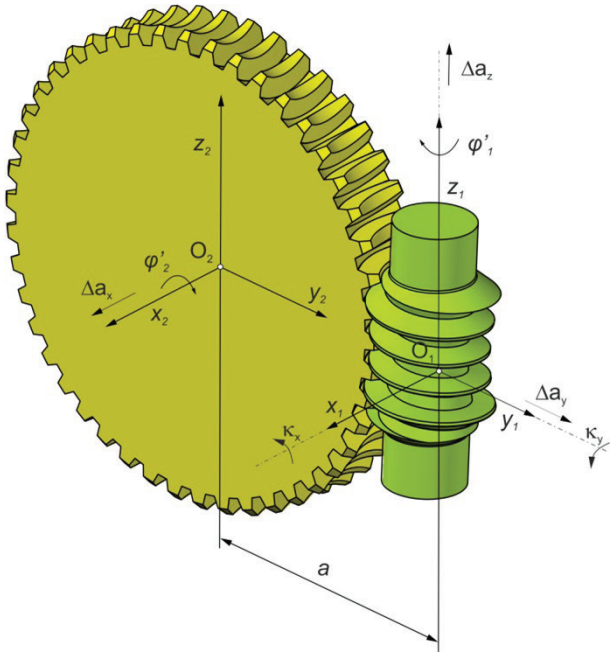

Figure 4. Kinematic system of the double enveloping worm gear.

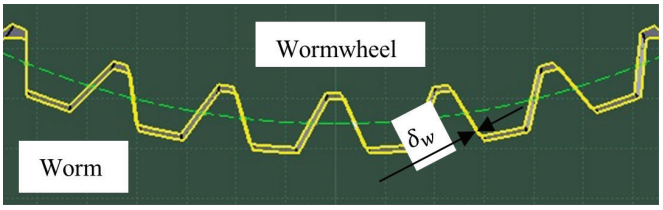

Figure 5. Interference of models presented in the center plane.

2. Determination of the Contact Pattern by Means of the Direct CAD Method

The CAD model of the globoid worm is presented in Figure 1. A tooth trace modification at the ends of the thread was taken into consideration. A globoid worm with a tooth trace modification at the ends of the thread should be characterized by an appropriate stress distribution at the entry of the meshing and a greater rigidity of the beginning of the thread.

The worm wheels of globoid gears can be machined in an enveloping or shaped manner. An hourglass hob will be similar to an hourglass worm in the case of an envelope processing. Moreover, appropriate clearances (tip clearance and circumferential backlash) should be provided to the worm geometry (so-called machining worm) used for modeling the worm wheel. The model of the machining worm is shown in Figure 2. In actual machining, the tooth surface of the worm wheel is shaped by a definite number of cutting edges of the hob cutter. A modeled tool can be imagined as a cutter in which an infinite number of cutting edges were made.

CAD model of the worm wheel is presented in Figure 3. Three zones are distinguished on the tooth flank surface of the worm wheel [4,11,19]. Region II is the envelope to the family of

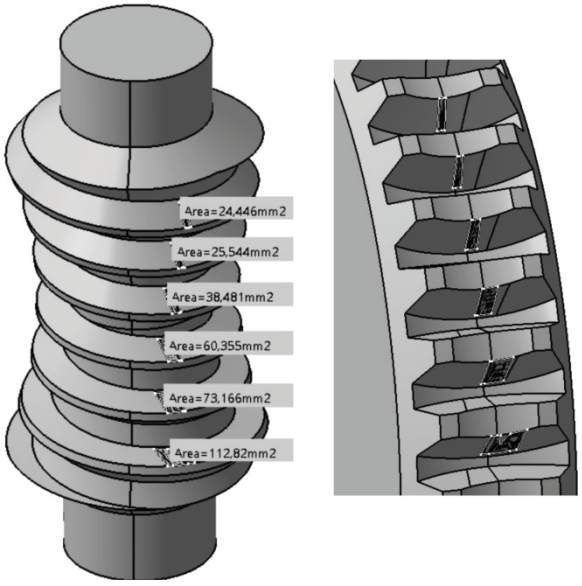

Figure 6. Temporary contact pattern presented on the model of worm and worm wheel.

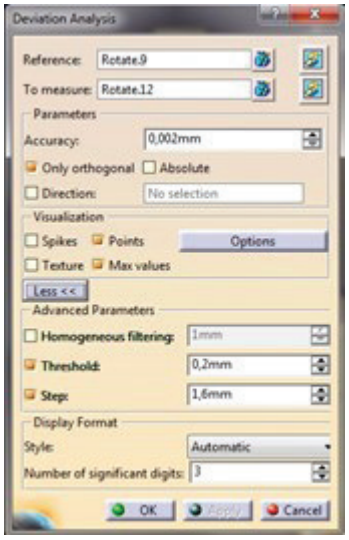

Figure 7. Window of *Deviation Analysis* function.

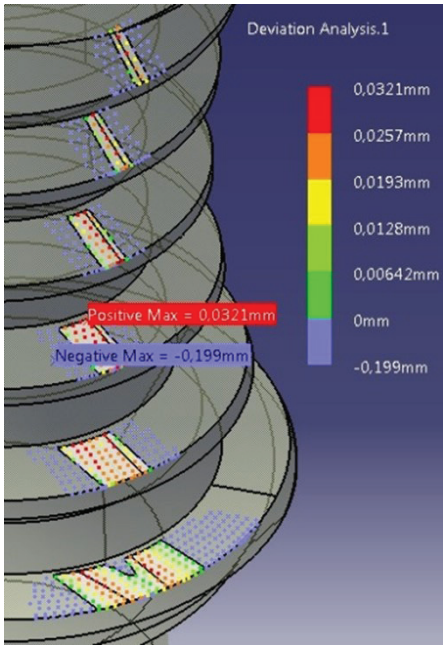

Figure 8. Measurement of the distances of flank surfaces of the interfered solids (with the flake element separated), presented on the worm model; exemplary results after introduction of deviation $\Delta a_x = -0.1\ mm$.

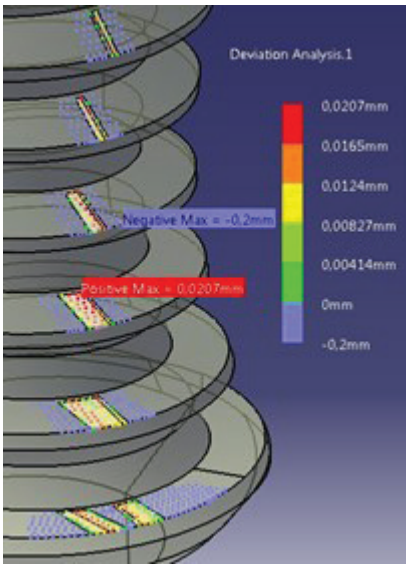

Figure 9. Measurement of the distances of flank surfaces after introducing the deviation Δa_x=–0.1 mm and additional worm wheel rotation obtaining the maximal interference of $\varphi_w \approx 0.02$ mm

contact lines of the globoid worm gear. Regions I and III are formed by the first cutting edge of the worm hob cutter [4,26]. One extreme cutting edge of the tool forms one side of the worm wheel tooth while the second edge forms the other flank. An analysis of the contact pattern in a CAD environment can be carried out during transmission by assembling the worm and worm wheel models for the transmission stage (Figure 4). As illustrated in Figure 4, the stationary coordinate systems $S_1(x_1,y_1,z_1)$ and $S_2(x_2,y_2,z_2)$ for worm and worm wheel were established, respectively. The worm rotates around the z_1 axis by the angle φ_1', opposite to the trigonometric direction. Then, the worm wheel rotates around the x_2 axis with the φ_2' angle,

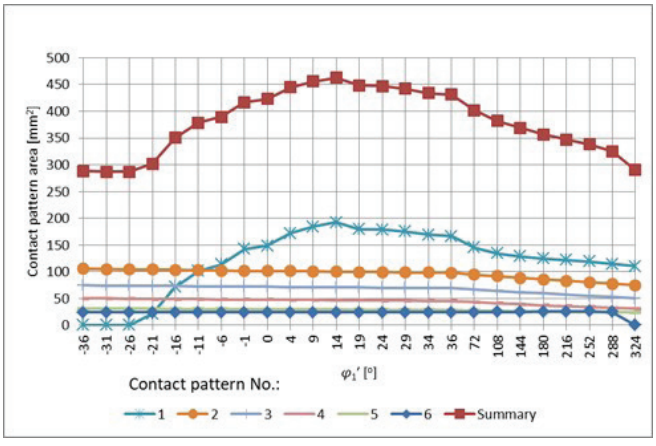

Figure 11. Changes of contact pattern surface area for the case I (horizontal axis without scale).

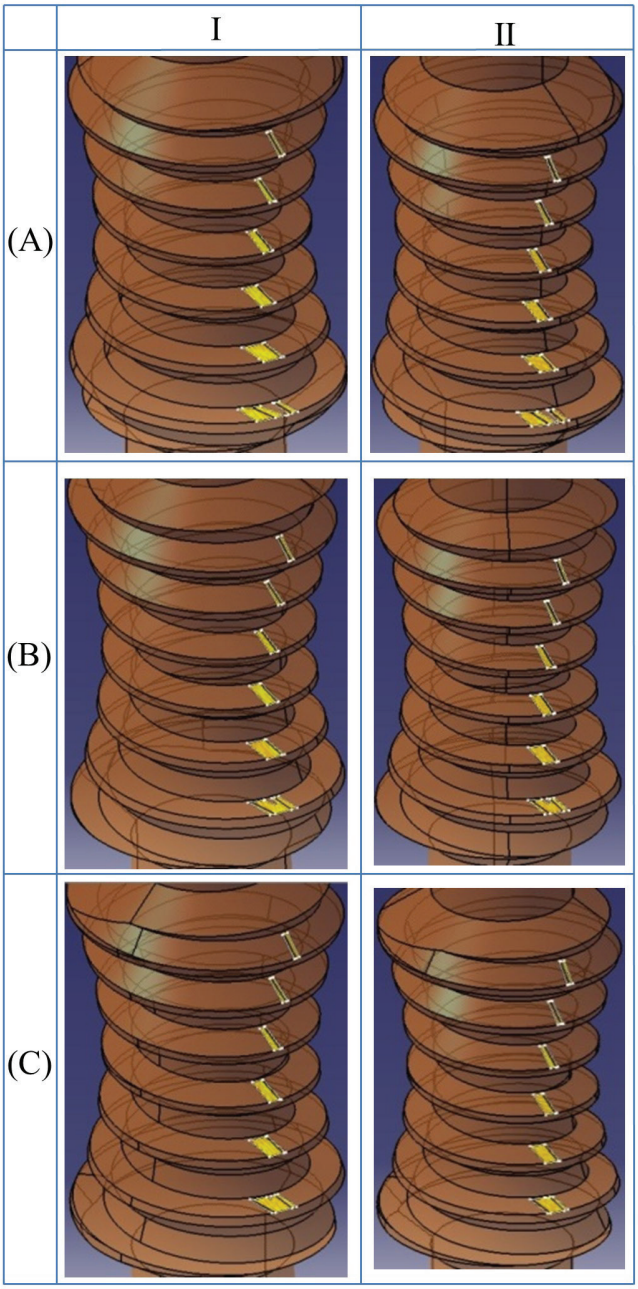

Figure 10. Temporary contact pattern presented by worm position: (A) φ_1'=0°, (B) φ_1'=144°, and (C) φ_1'=216°.

as well as opposite to the trigonometric direction (in the case of using a left hand thread worm). For ideal gear, assembling errors and manufacturing errors of the body (settings concerning the gear pair) are excluded, together with elastic deformations of shafts and bearings. Parameterization of the relative rotation of worm and worm wheel were introduced. Additionally, the worm wheel model has to be rotated by the

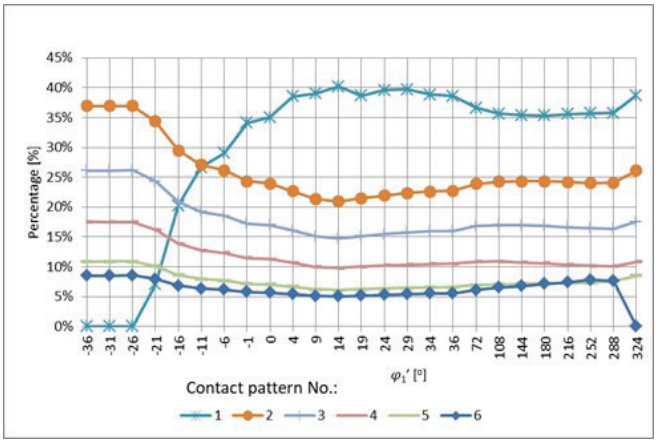

Figure 12. Percentage share of the contact pattern in transferring the load for the case I (horizontal axis without scale).

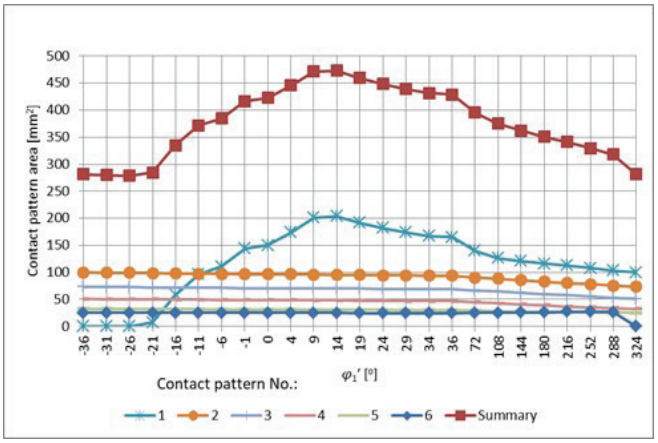

Figure 13. Changes of contact pattern surface area for the case II (horizontal axis without scale).

angle relative to the x_2, so as to interfere into the worm tooth by the given value δ_w (Figure 5). By simulating gear rotation (Figure 4), the models rotate in fixed discrete steps, whose movements will be based on the gear ratio. For a given gear position, the intersection of the worm and worm wheel is determined (Figure 6). The surface area of contact pattern can be determined directly by measuring the areas of flake elements (Figure 6) or analyzing the interference volume [27]. It may be assumed that the ratio of interference volume to the areas of flake elements is approximately constant [27].

The tooth contact analysis can be investigated for the whole cycle of worm rotation. Based on this method, it is possible to analyze the shape of the contact pattern and perform graphical characteristic of the contact area size depending on worm position. CAD model of the globoid worm considers the whole thread length, which allows a complete analysis of the correctness of meshing.

Possible shifts of the worm in relation to the axis $y_1(\Delta a_y)$ and $z_1(\Delta a_z)$, as well as shift of the worm wheel in relation to the axis $x_2(\Delta a_x)$ were assumed for the gear. Angular deviations in relation to the worm axis were introduced, i.e., in relation to the axis x_1—the deviation κ_x, and in relation to the axis y_1—the deviation κ_y (Figure 4) are introduced. Also, possible translations and rotations of worm and worm wheel CAD models were introduced. The considered transformations enable us to analyze several deviations simultaneously. The models were completed with relative worm and worm wheel rotation resulted from gear kinematics. For the case of the worm wheel model, an additional rotation parameter δ_w in relation to the x'_2 axis is introduced, which is responsible for interference the models by the value of δ_w, as in Figure 5. After taking into account any mounting deviation in the CAD model, the value of the parameter δ_w may be estimated in the CATIA system by using the function of *Deviation Analysis* from

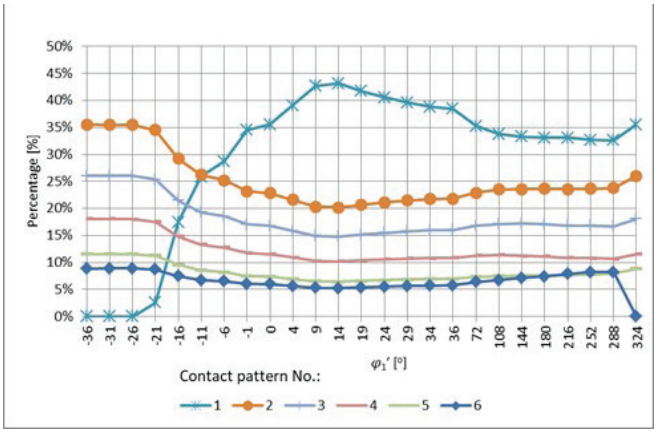

Figure 14. Percentage share of the contact pattern in transferring the load for the case II (horizontal axis without scale).

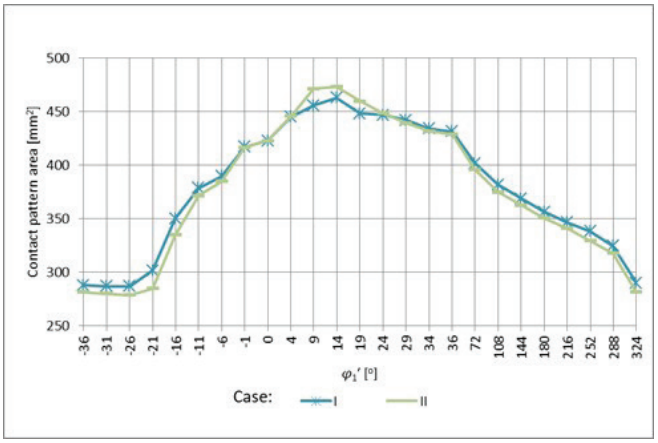

Figure 15. Summary contact pattern area for the case I and II (horizontal axis without a scale).

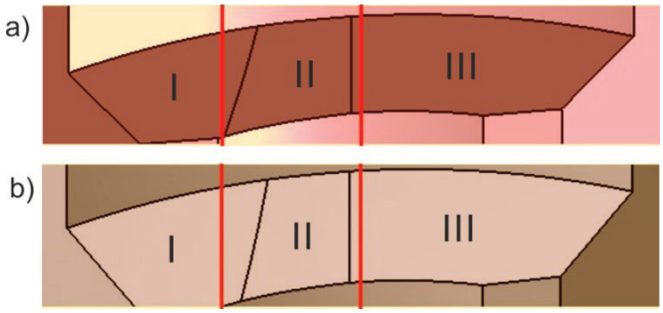

Figure 16. Worm wheel tooth side fragment with the marked regions I–III: (A) for $(a_n = 20°)$, (B) for $(a_n = 25°)$.

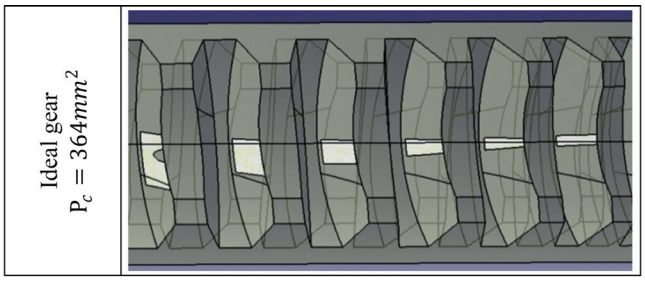

Figure 17. Temporary contact pattern of ideal gear for worm position of φ'_1=144°.

the module of *Quick Surface Reconstruction*. The reference plane (*Reference*) (e.g., worm wheel) and measured (*To measure*) (e.g., *worm*) is defined. The analysis takes place by measuring the distance of the measured and reference planes in the direction perpendicular to the reference plane. The measurement step (*Step*) is defined. Additionally, the point visualization method was selected with indication of the maximal values and the limit value of the displayed results (Figure 7).

The presented points with positive values define the areas of solids that interfere (Figure 8). On the basis of the analysis of the distance of area, it is possible to estimate the angle that the worm wheel should be rotated in relation to the x'_2 axis, so that the interference of the models takes the assumed value of δ_w, with the accuracy of up to 0.001 mm. Figure 9 presents exemplary results of area distances after correction of the worm wheel rotation, obtaining the maximal assumed interference of solids δ_w, with the assumed accuracy.

3. The Analysis of the Globoid Worm Gear Contact Pattern Results Done by Means of the CAD Direct Method

The analyses of the contact pattern by means of the CAD direct method were done by assuming the marker thickness as approximately 0.02 mm for the data presented in the Table 1.

Figure 10 shows temporary contact pattern presented for the cases I and II for the given worm position.

Based on the results of temporary contact pattern, it is possible to analyze the shape of the contact pattern and perform graphical characteristic of the contact area size depending on worm position (Figures 11 and 13). Assuming that the area of the contact pattern in a given gear position reflects their proportion of share in the load transfer, graphs in Figures 12 and 14 are made. Please note that the horizontal

Table 1. Data of analyzed gear pair

Parameter	Worm	Worm wheel
Normal module [mm]	$m_n = 7.1365$	
Number of threads in worm/number of teeth in gear	$z_1 = 1$	$z_1 = 47$
Worm pitch diameter in transverse plane/Gear pitch diameter in central plane [mm]	$d_{w1} = 70$	$d_{w2} = 330$
Worm throat diameter in transverse plane/Gear throat diameter in central plane [mm]	$d_{a1} = 80.09$	$d_{a2} = 340.09$
Worm root diameter in transverse plane/Gear root diameter in central plane [mm]	$d_{f1} = 57.7$	$d_{f2} = 317.67$
Effective worm thread length/Gear face width [mm]	$b_{1eff} = 135$	$b_2 = 57$
Normal pleasure angle [°]	$a_n = 20°$ (case I)	
	$a_n = 25°$ (case II)	
Center distance [mm]	$a = 200$	

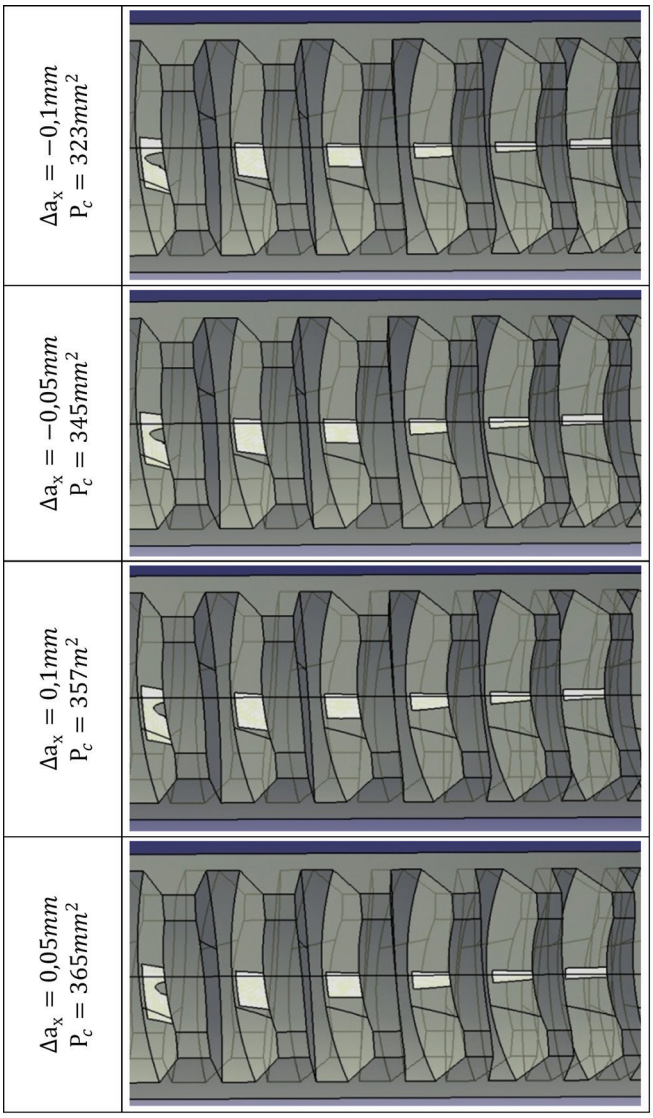

Figure 18. Temporary contact pattern of the gear with deviation, Δa_x.

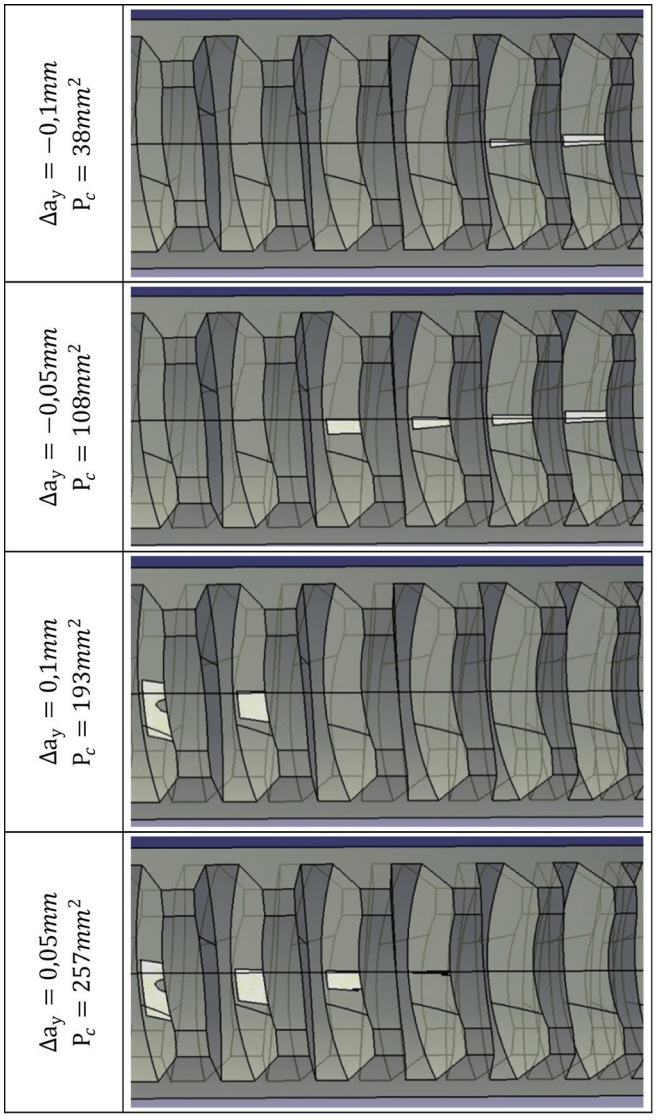

Figure 19. Temporary contact pattern of the gear with deviation, Δa_y.

axis of the graphs is not drawn to the scale and vertical axis represents the contact pattern surface area at the beginning of worm thread when in mesh.

Figure 15 shows the summary contact pattern surface areas when compared for case I and II.

The summary contact pattern for the significant range of worm rotation is higher for the first case $(a_n = 20°)$, due to greater width of region II of worm wheel tooth flank (Figure 16A), which results from the generating process. For the second case $(a_n = 25°)$ where the width of region II of worm wheel tooth flank is narrower (Figure 16B), the contact pattern is greater by entrance the begging of worm thread in mesh.

4. Analysis of the Influence of Mounting Deviations on the Contact Pattern Done by Applying the CAD method

The analysis of the influence of mounting deviations was performed for case I for one gear position. Maximal interference of models equal to or approximate (with the accuracy of 0.001 mm) value of 0.020 mm was assumed. Figure 17 shows temporary contact pattern of an ideal gear for worm position of $\varphi'_1 = 144°$ and defined surface area P_c. The analysis of temporary contact pattern with the introduced deviation for the same position of the φ'_1 worm model will be related to this result.

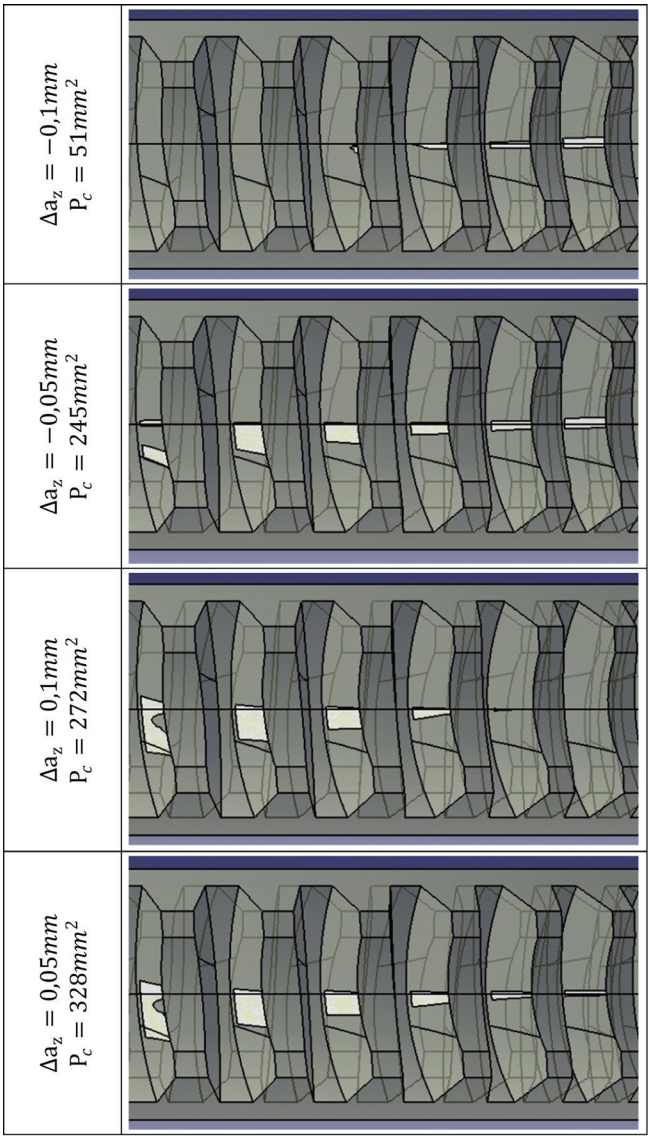

Figure 20. Temporary contact pattern of the gear with deviation Δa_z.

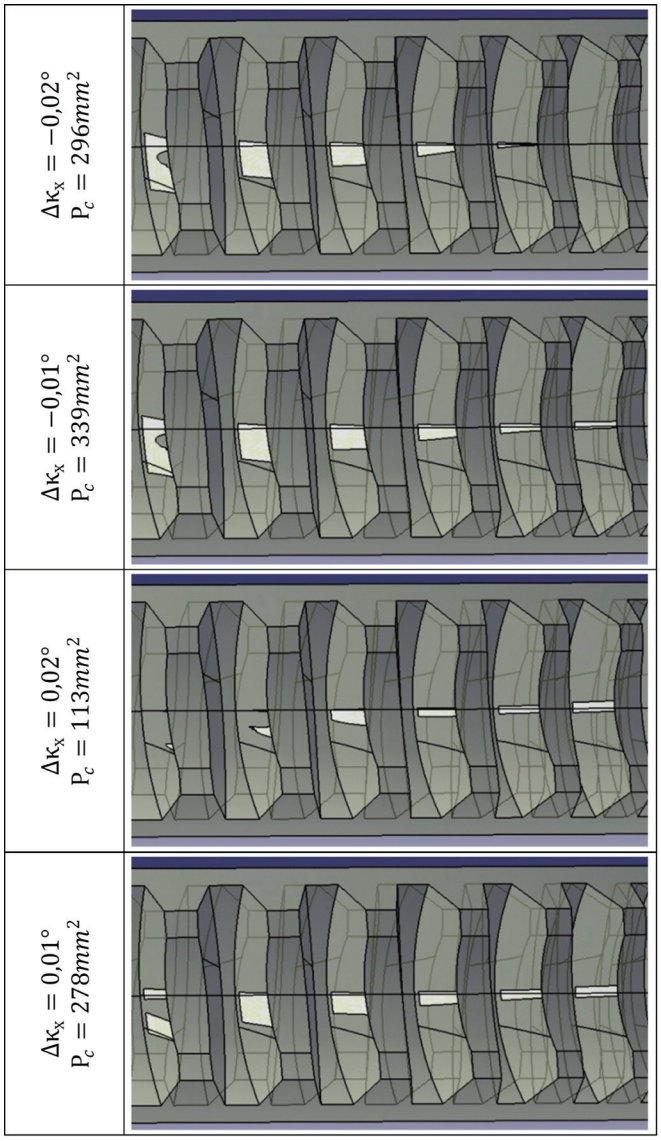

Figure 21. Temporary contact pattern of the gear with deviation $\Delta\kappa_x$.

Figure 18 presents a temporary contact pattern after considering deviation Δa_x.

The gear does not demonstrate significant changes in the shape and position of the temporary contact pattern for the deviation, Δa_x. The contact pattern surface area decreases together with higher deviation value. The gear is more susceptible to negative Δa_x deviations.

Temporary contact pattern considering deviation Δa_y is presented in Figure 19.

The gear is highly susceptible to center distance error. Further, some of the temporary contact patterns diminish together with the center distance errors. Because of negative deviation, the temporary contact patterns disappear from the side of entrance of worm thread in mesh. By increasing of center distance, the temporary contact patterns disappear from the opposite side. The shape changes and the surface area of temporary contact patterns in both cases significantly decrease, while the gear is more susceptible to negative Δa_y deviation.

Temporary contact pattern after considering deviation Δa_z is presented in Figure 20.

On the basis of the analysis in Figure 20, it can be seen that the gear is susceptible to deviation Δa_z, especially for negative values. So, the first temporary contact patterns diminish. Thus,

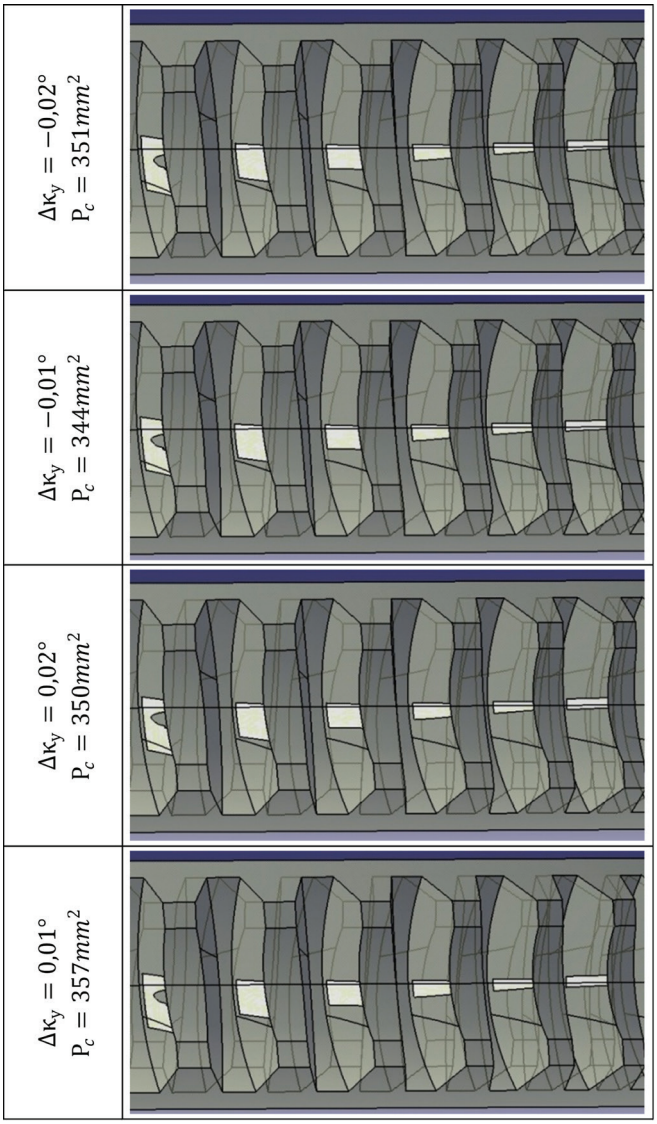

Figure 22. Temporary contact pattern of the gear with deviation $\Delta\kappa_y$.

the area of temporary contact pattern decreases significantly, whereas the end contact patterns reduce for positive deviations. Temporary contact pattern after considering deviation $\Delta\kappa_x$ is presented in Figure 21.

Positive deviation $\Delta\kappa_x$ distorts the shape and size of temporary contact patterns, which leads to the reduction of contact patterns at first. Negative deviation $\Delta\kappa_x$ leads to decrease of the end contact patterns. Among the analyzed deviations $\Delta\kappa_x$, those with positive values are less beneficial.

Temporary contact pattern after considering deviation $\Delta\kappa_y$ is presented in Figure 22.

The gear does not show significant changes in the shape and position of the temporary contact pattern for the deviation of $\Delta\kappa_y$.

5. Conclusion

The presented method of determining geometric contact pattern obtained by means of the direct CAD method for globoid worm gear allows establishing its shape and area. The surface area of contact pattern can be determined directly by measuring the areas of flake elements or analyzing the interference volume. The tooth contact analysis can be performed for all cycle of worm rotation. Based on the results of temporary contact pattern, it is possible to analyze the shape of the contact pattern and perform graphical characteristic of the contact area size depending on worm position. Graphical characteristics allow analyzing the single contact patterns or the summary. Additional diagrams can be performed based on the assumption that the area of the contact pattern in a given gear position refer to their proportional share in the load transfer. Based on presented method, a complete analysis of the correctness of gear meshing can be obtained. If the worm or worm wheel is incorrectly designed in terms of the geometry, the meshing simulation of CAD models can indicate the collision.

Contact pattern analyses performed in CAD environment show that the globoid worm gear is characterized by multi-tooth contact. The surface area of the first contact pattern during the whole cycle of worm rotation is the greatest, and the contact pattern is smaller for each subsequent fragment of helical surface. The first contact region has significant influence on load transfer. Therefore, it is important to introduce a modification of the tooth trace beyond the range of effective worm length. Then, the beginning of the thread should be characterized by a more favorable or appropriate stress distribution at the time of entry for the meshing.

The pressure angle has influence on tooth contact pattern surface area. For the case where $(a_n = 20°)$, the total contact pattern in the major range of worm rotation is bigger due to greater width of region II of worm wheel tooth flank. For the pressure angle $(a_n = 25°)$ where the width of region II of worm wheel tooth flank is narrower, the contact pattern is greater by entrance the begging of worm thread in mesh.

Among the analyzed deviations, it is found that it is possible to correct are the assembling ones, i.e., Δa_x—by means of worm wheel axial positioning and Δa_z—by means of worm axial positioning. It is observed that incorrect worm setting can have significant influence on the size and shape of temporary contact patterns and, thus, the gear load capacity. The most unfavorable is the deviation Δa_y resulting from not keeping the center distance appropriately. It cannot be corrected and the contact pattern size is significantly reduced. Jamming can occur with negative deviations Δa_y for gears with very small circumferential backlash. Further, the gear is more sensitive to the deviation Δa_x among the angular deviations. It can be

found that the double-enveloping worm gear drive is sensitive to tolerances. It needs precise manufacturing and accurate alignment.

Modeling in a CAD environment is particularly useful for engineers designing such gears. They are usually accustomed and well-versed users of CAD systems so that they can build the gear model themselves and perform analyses of the geometrical contact pattern in a CAD environment. The presented method of determining geometric contact pattern allows to performing meshing analyses of gears prior to their manufacturing.

References

[1] I. DUDAS: The theory and practice of worm gear drives. Penton Press, London 2000.

[2] W.P. CROSHER: Design and Application of the Worm Gear. ASME Press, New York 2002.

[3] F.L. LITVIN: Development of gear technology and theory of gearing. NASA, Levis Research Center, 1999.

[4] F.L. LITVIN, A. FUENTES: Gear geometry and applied theory. Cambridge University Press 2004.

[5] L. DUDÁS: New technology for manufacturing quasi-globoid worm gearings. *Mater. Sci. Eng*., 448(2018), 012035.

[6] Y. CHEN, et al.: Development and classification of worm drive. The 14th IFToMMWorld Congress in Taiwan 2015.

[7] K.Y. CHEN, CH.B. TSAY: Mathematical model and worm wheel tooth working surfaces of the ZN-type hourglass worm gear set. *Mech. Mach. Theory*., 44(2009), 1701-1712.

[8] L.V. MOHAN, M.S. SHUNMUGAM: Geometrical aspects of double enveloping worm gear drive. *Mech. Mach. Theory*., 44(2009), 2053-2065.

[9] CH. HUAI, Y. ZHAO: Variable height modification of TA worm drive. *Proc. Inst. of Mech. Eng., Part C: J. Mech. Eng. Sci*., 233(2018), 095440621875726.

[10] F. HE, Z. SHI, B. YU: Effects of tooth surface modification on planar double-enveloping hourglass worm gear drives. *J. Adv. Mech. Des., Syst., Manuf*., 12(2018), JAMDSM0040-JAMDSM0040.

[11] Y. ZHAO, Y. ZHANG: Computing method for induced curvature parameters based on normal vector of instantaneous contact line and its application to Hindley worm pair. *Adv. Mech. Eng*., 9(2017), 168781401772188.

[12] Y. ZHAO, Y. ZHANG: Novel methods for curvature analysis and their application to TA worm. *Mech. Mach. Theory*., 97(2016), 155-170.

[13] V. SIMON: A new type of ground double enveloping worm gear drive. Proc. ASME 5th Int. Power Transm. and Gearing Conf., Chicago, 1989, 281-288.

[14] V. SIMON: Double enveloping worm gear drive with smooth gear tooth surface. Proc. Int. Conf. on Gearing, Zhengzhou, China, 1988, 191-194.

[15] S. LAGUTIN, E. GUDOV, B. FEDOTOV: Manufacturing and load rating of modified globoid gears. *Balkan J. Mech. Transm. (BJMT)*. 1(2011), 45-53.

[16] A.V. SUTYAGIN, L.S. MAL'KO, I.V. TRIFANOV: More efficient machining of globoid worm gears. *Rus. Eng. Res*., 35(2015), 623-627.

[17] Y. CHEN, et al.: Study on the spur involute gear meshing with planar enveloping hourglass worm based on local conjugate. *Proc. Inst. Mech. Eng., Part C: J. Mech. Eng. Sci*., 232(2017), 095440621770821.

[18] Y. ZHAO, CH. HUAI, Y. ZHANG: Compound modification of globoidal worm drive with variable parameters. *Appl. Math. Model*., 50(2017), 17-38.

[19] P. POLOWNIAK, M. SOBOLAK: Mathematical description of tooth flank surface of globoidal worm gear with straight axial tooth profile. *Open Eng*., 7(2017), 407-415.

[20] Z. LIU, et al.: A novel CNC machining method for enveloping surface. *Int. J. Adv. Manuf. Technol*., 85(2015), 779-790.

[21] Z. LIU, et al.: Digitization modelling and CNC machining for cone-generated double-enveloping worm drive. *Int. J. Adv. Manuf. Technol*., 95(2018), 3393-3412.

[22] A.L. KHEYFETS: Geometrically accurate computer 3D models of gear drives and hob cutters. *Procedia Eng*., 150(2016), 1098-1106.

[23] A.L. KHEYFETS: Programming while construction of engineering 3D models of complex geometry. *Mat. Sci. Eng*., 262(2017), 012111.

[24] P. POŁOWNIAK, M. SOBOLAK: Modelling a globoid worm in CAD environment. *Miesięcznik Naukowo – Techniczny Mechanik*, 1(2015), 71-74. (in Polish).

[25] P. POŁOWNIAK, M. SOBOLAK: Modelling a globoid worm wheel in CAD environment. *Miesięcznik Naukowo – Techniczny Mechanik*, 3(2015), 250-252. (in Polish).

[26] P. POŁOWNIAK, M. SOBOLAK: Effect of the extreme hob edge on generation of the worm wheel tooth flank. *Miesięcznik Naukowo – Techniczny Mechanik*, 7(2016), 625–627. (in Polish).

[27] M. SOBOLAK: Analysis and synthesis of mating gear tooth surface by discrete methods. Rzeszow University of Technol. Publ., Rzeszow, 2006. (in Polish).

[28] M. BATSCH, et al.: Measurement and mathematical model of convexo-concave Novikov gear mesh. *Measurement*, 125(2018), 516-525.

[29] M. SOBOLAK, et al.: Application of polymeric materials for obtaining gears with involute and sinusoidal profile. *Polimery*, 7-8(2020), 563-567.